Antiviral Research 167 (2019) 110–116

Contents lists available at ScienceDirect

Antiviral Research

journal homepage: www.elsevier.com/locate/antiviral

Structural and pharmacological evaluation of a novel non-nucleoside reverse transcriptase inhibitor as a promising long acting nanoformulation for treating HIV

Shalley N. Kudalkar[a,b,1], Irfan Ullah[c,1], Nicole Bertoletti[a,b], Hanna K. Mandl[d], José A. Cisneros[e], Jagadish Beloor[c], Albert H. Chan[a,b], Elias Quijano[d], W. Mark Saltzman[d], William L. Jorgensen[e], Priti Kumar[c], Karen S. Anderson[a,b,*]

[a] Department of Pharmacology, Yale University School of Medicine, New Haven, CT 06520-8066, USA
[b] Department of Molecular Biophysics and Biochemistry, Yale University School of Medicine, New Haven, CT 06520-8066, USA
[c] Department of Internal Medicine, Section of Infectious Diseases, Yale University School of Medicine, New Haven, CT 06520, USA
[d] Department of Biomedical Engineering, Yale University, New Haven, CT 06511, USA
[e] Department of Chemistry, Yale University, New Haven, CT 06520-8107, USA

ARTICLE INFO

Keywords:
HIV-1
Non-nucleoside reverse transcriptase inhibitor
Long-acting nanoformulation
Pharmacokinetic studies
Mice model
X-ray crystallography

ABSTRACT

Combination antiretroviral therapy (cART) has been proven effective in inhibiting human immunodeficiency virus type 1 (HIV-1) infection and has significantly improved the health outcomes in acquired immune deficiency syndrome (AIDS) patients. The therapeutic benefits of cART have been challenged because of the toxicity and emergence of drug-resistant HIV-1 strains along with lifelong patient compliance resulting in non-adherence. These issues also hinder the clinical benefits of non-nucleoside reverse transcriptase inhibitors (NNRTIs), which are one of the vital components of cART for the treatment of HIV-1 infection. In this study, using a computational and structural based drug design approach, we have discovered an effective HIV -1 NNRTI, compound I (Cmpd I) that is very potent in biochemical assays and which targets key residues in the allosteric binding pocket of wild-type (WT)-RT as revealed by structural studies. Furthermore, Cmpd I exhibited very potent antiviral activity in HIV-1 infected T cells, lacked cytotoxicity (therapeutic index > 100,000), and no significant off-target effects were noted in pharmacological assays. To address the issue of non-adherence, we developed a long-acting nanoformulation of Cmpd I (Cmpd I-NP) using poly (lactide-coglycolide) (PLGA) particles. The pharmacokinetic studies of free and nanoformulated Cmpd I were carried out in BALB/c mice. Intraperitoneal administration of Cmpd I and Cmpd I-NP in BALB/c mice revealed prolonged serum residence time of 48 h and 30 days, respectively. The observed serum concentrations of Cmpd I in both cases were sufficient to provide > 97% inhibition in HIV-1 infected T-cells. The significant antiviral activity along with favorable pharmacological and pharmacokinetic profile of Cmpd I, provide compelling and critical support for its further development as an anti-HIV therapeutic agent.

1. Introduction

Worldwide, antiretroviral therapy has markedly improved the morbidity and mortality associated with human immunodeficiency virus (HIV)-1 infection. Patients receiving combination antiretroviral therapy (cART) show significant reduction in hospitalizations and improved survival rates. One of the vital components of cART for the treatment of HIV-1 infection is non-nucleoside reverse transcriptase inhibitors (NNRTIs), which disrupt the normal functions of HIV-1 reverse transcriptase (RT) via binding to NNRTI binding pocket (NNIBP)

Abbreviations: HIV, Human immunodeficiency virus; HIV-RT, HIV reverse transcriptase; NNRTI, Non-nucleoside reverse transcriptase inhibitor; EC_{50}, Half maximal effective concentration of a compound; IC_{50}, Half maximal inhibitory concentration of a compound; HPLC, High performance liquid chromatography; PK, Pharmacokinetics; C_{max}, The maximum concentration of a drug observed in serum after its administration; T_{max}, The time taken to reach C_{max}; AUC, A plot of concentration of drug in blood plasma against time; CL, Clearance; NP, Nanoparticle; PKs, Pharmacokinetics

* Corresponding author. Department of Pharmacology, Yale University School of Medicine, New Haven, CT 06520-8066, USA.
E-mail address: karen.anderson@yale.edu (K.S. Anderson).

[1] S.N.K. and I.U contributed equally to this work.

https://doi.org/10.1016/j.antiviral.2019.04.010
Received 3 April 2019; Accepted 23 April 2019
Available online 26 April 2019
0166-3542/

close to the polymerase active site (Kohlstaedt et al., 1992). In 1996, US Food and Drug Administration approved Nevirapine (NVP) as the first NNRTI for the treatment of HIV-1 infection, followed by delavirdine (1997), efavirenz (EFV) (1998), etravirine (ETV) (2008), and rilpivirine (RPV) (2011).

Although these NNRTIs are key components of effective cART regimens, their effectiveness is often outweighed by their poor pharmacokinetic properties, dose-limiting toxicities, and requirement of chronic treatment (Delaugerre et al., 2001; Huang et al., 2015; Rhee et al., 2015). These properties increase the chances of developing drug resistant mutations and non-adherence in patients receiving cART. Additionally, other factors like cost of medication, lack of social support, high dosing, and wide fluctuations between peak and trough levels between dosing interval reduces adherence. For instance, use of RPV is restricted in patients with viral loads of < 100,000 copies due to the dose-limiting cardiotoxicity caused by inhibition of hERG-ion channel (Bowes et al., 2012). Additionally, EFV's low genetic barrier to resistance combined with various side effects in patients makes it very hard to achieve required level of adherence (de Waal et al., 2013; Riddler et al., 2008).

In continuous efforts to develop next-generation NNRTIs with improved antidrug resistance, pharmacokinetics and toxicity profiles we have used computational and structure-based drug design to discover a class of inhibitors known as catechol diethers (Lee et al., 2016; Lee et al., 2014; Lee et al., 2015; Lee et al., 2013). One of the most potent inhibitors from this series is Cmpd I (Fig. 1). Cmpd I showed significant potency along with remarkable efficacy on clinically relevant drug resistant strains of HIV-1, and lack of cytotoxicity as described previously (Lee et al., 2016; Lee et al., 2014; Lee et al., 2015; Lee et al., 2013). In the current study, we further explored Cmpd I as a potential anti-HIV drug candidate by dissecting the molecular mechanism through biochemical and structural studies as well as investigating Cmpd I's in vitro and in vivo pharmacological profiles.

To reduce dosing frequency and to improve the quality of life of HIV/AIDS patients by tackling non-adherence, long-acting parenteral therapeutics containing cART are being developed and tested for their efficacy in animal models (Gao et al., 2018; Mandal et al., 2018). Hence, Cmpd I was further developed into a long-acting nanoformulation (Cmpd I-NP) using a biodegradable polymer, poly (lactide-coglycolide) (PLGA), that has been approved by the FDA for drug delivery and other applications. The pharmacokinetic profiles of free Cmpd I and Cmpd I-NP were then investigated in BALB/c mice.

2. Materials and methods

2.1. Chemicals and synthesis of compound I

Poly (d,l lactic-*co*-glycolic acid), 50:50 with inherent viscosity 0.55–0.75 dl/g, was purchased from DURECT Corporation (Birmingham, AL). Cmpd I was synthesized as detailed previously (Lee et al., 2014).

2.2. Animals

Six-to eight-week-old female BALB/c mice from Jackson laboratories were used. All mice were housed in cages containing water, food and bedding. All procedures were approved by Yale University Animal Care and Use Committee.

2.3. Inhibition assay with Pico Green and solubility measurements for Cmpd I

Inhibition assays were carried out with the PicoGreen Enzcheck Reverse Transcriptase Assay Kit (Life Technologies) as described previously (Gray et al., 2015). The compound solubility was measured using a shake-flask procedure as described previously (Bollini et al., 2013; Lee et al., 2013; Lee et al., 2013).

2.4. Measurement of the inhibitory activity of Cmpd I-NP in infected TZM-bl cells

The in vitro anti- HIV-1 activity from serum samples collected at various time intervals after intraperitoneal injection of free and nanoformulated Cmpd I was determined using a luciferase reporter gene assay as described previously (Kudalkar et al., 2017).

2.5. In vitro pharmacological profiling

In vitro pharmacological profiling of Cmpd I and efavirenz was carried out by Eurofins Groups (Cerep and Eurofins Panlabs) in a panel of enzyme and radio-ligand assays with 34 targets as described previously (Kudalkar et al., 2017).

2.6. Expression, purification and crystallization of the recombinant RT52A protein

Recombinant RT52A enzyme was expressed and purified as described previously (Das et al., 2008; Frey et al., 2012). Crystals of RT52A in complex with Cmpd I were prepared using similar methods as already described (Frey et al., 2012; Kudalkar et al., 2017).

2.7. Data collection, processing and structure determination and refinement

Crystals of sufficient quality were collected at APS on beam line 24-ID-E through NE-CAT. The data collection of protein-Cmpd I complex (PDB ID code: 6OE3) was achieved at a wavelength of 0.98 Å and a temperature of 100 K on a silicon Pilatus HF-4M pixel detector. Data sets for the best diffracting crystals were indexed, processed and scaled with XDS (Kabsch, 2010). Phases were solved by molecular replacement with the program PHASER MR (McCoy et al., 2007) from the CCP4 suite (Collaborative Computational Project, 1994) using the

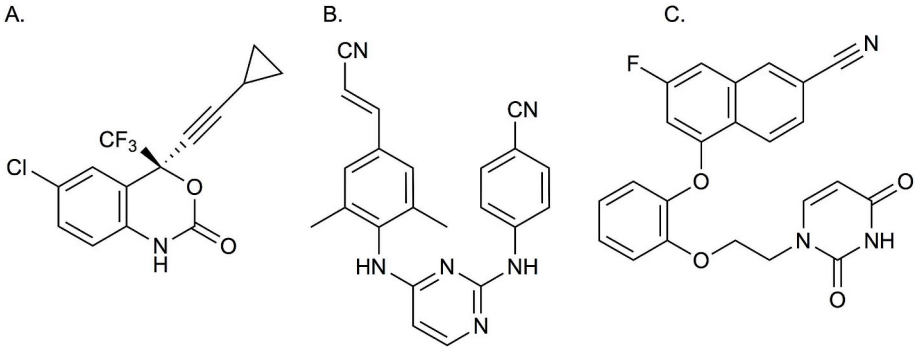

Fig. 1. Chemical structures of (A) efavirenz, (B) rilpivirine, and (C) Cmpd I.

Table 1
HIV-RT inhibitory activity (IC_{50} and EC_{50} in nM), computed C log P, experimental aqueous solubility (in μg/ml) at pH 6.5, and cell cytotoxicity (in μM). Data are the mean ± S.D. values from three different experiments involving triplicate measurements.

Compounds	IC50 WT (nM)	EC_{50} WT (nM)	ClogP	S (μg/ml)	CC_{50} (μM)
Cmpd I[a]	4.8 ± 1.1	1.1	3.59	9.1[a]	> 100
Rilpivirine	1.5 ± 0.4	0.67[b]	5.75	0.02[c],0.24[d]	8
Efavirenz	41 ± 2	2[e]	4.67[b]	68[b]	15

[a] Lee et al. (2014).
[b] Kudalkar et al. (2017).
[c] Janssen et al. (2005), pH 7.
[d] Sun et al. (2012), PH 7.4.
[e] King et al. (2002).

structure 4H4M as a search model. A subset corresponding to 5% of all reflections were omitted during refinement and used for the calculation of R_{free}. Model building was performed in Coot (Emsley and Cowtan, 2004; Emsley et al., 2010) and refinement using PHENIX refine version 1.14–3260 (Adams et al., 2010). Cmpd I SMILE codes were created with Molinspiration v2018.10 (http://www.Molinspiration.com), built with the Grade Web Server (Smart et al., 2011) and Cmpd I restraints were generated with eLBOW (Moriarty et al., 2009). Cartesian simulated annealing, applying default parameters, was used as a first refinement step. Subsequently, refinement of XYZ coordinates, occupancies and individual B-factors were alternated with structural adaption until the model was readily built and gave the best possible explanation of the electron density, acceptable R-factors, geometry statistics, and Ramachandran statistics were achieved. Crystallography programs were compiled by SBGrid (Morin et al., 2013).

2.8. Fabrication of Cmpd I loaded nanoparticles (Cmpd I-NPs)

PLGA nanoparticles were formulated by a single-emulsion solvent evaporation technique (Kudalkar et al., 2018; Le Thi Mai et al., 2009). For the 10 wt % Cmpd I-loaded formulation, 5.0 mg of compound I was dissolved in 0.250 ml of dimethylformamide, then added to 50 mg of 30–55 kDa PLGA in 1 ml methylene chloride to further co-dissolve overnight (for a concentration of 50 mg/ml).

To create a single-emulsion, the dissolved polymer solution was added dropwise to 1.25% polyvinyl alcohol under vortex followed by three sonications (10 s each) using a probe sonicator (38% amplitude). The final mixture was added to 25 ml of 0.3% polyvinyl alcohol, and stirred at room temperature for 3 h to evaporate the methylene chloride and DMF. The nanoparticles were then collected and transferred to a VWR 20 K Ultra High Performance centrifugal filter unit and washed three times at 16,000 g at 4 °C for 15 min with water. After the final wash, nanoparticles were resuspended in trehalose as a cryoprotectant at 100% (wt/wt) before lyophilization.

2.9. Characterization of Cmpd I loaded nanoparticles (Cmpd I-NPs)

NP size, polydispersity index (PDI) and zeta (ζ) potential were measured as described previously (Kudalkar et al., 2018). Reverse-phase high-pressure liquid chromatography (HPLC) was used to measure drug loading (DL) as detailed previously (Kudalkar et al., 2018), which is defined as the measured mass of Cmpd I per mass of PLGA-NP, and encapsulation efficiency (EE), which is defined as the ratio of the compounds loaded to the total drugs used for fabricating the nanoparticles (equations (1) and (2))

$$\text{Drug loading (DL)}(\%) = \frac{\text{mass of compound I in nanoparticles}}{\text{total mass of nanoparticles}} * 100$$

$$\text{Encapsulation efficiency (EE)}(\%) = \frac{\text{mass of drug in nanoparticles}}{\text{mass of polymer used in formulation}} * 100$$

2.10. Pharmacokinetic studies in BALB/c mice

To determine dose-dependent serum drug concentrations, the in vivo pharmacokinetics of free Cmpd I and Cmpd I-NP were investigated on BALB/c mice obtained from Jackson Laboratory. BALB/c mice were randomly divided into two groups containing 3 mice each. One group of mice was injected intraperitoneally (i.p.) with a single 100 mg/kg dose of free Cmpd I suspended in sterile saline solution containing 10% Tween 80. The second group was injected intraperitoneally with single 125 mg/kg Cmpd I-NP dose suspended in sterile saline solution. The blood samples were collected at predetermined time points from the ocular venous plexus by retro-orbital venipuncture and used for subsequent analysis as detailed previously.

2.11. Pharmacokinetic analyses

The data were plotted as concentration as a function of time using PRISM 7.0 (GraphPad Software Inc,LaJolla, CA). The predicted area under the curve (AUC) of the concentration of drug in blood plasma against time ($AUC_{predicted}$) was calculated based on the linear trapezoid method (Bourget and Delouis, 1993). The maximum concentration (C_{max}) of a drug observed in serum after its administration and the maximum time (T_{max}) taken to reach C_{max} were also calculated from the concentration-time curve. The total body clearance (CL) value was obtained by the following equation (Ratain and Plunkett, 2003):

$$CL = \text{Dose}/AUC_{0-last} \quad (1)$$

3. Results and discussion

The molecular mechanism of inhibition of HIV-1 RT Cmpd I was investigated by the biochemical and structural studies. As illustrated in Table 1, very potent inhibition of RT (IC_{50} = 4.8 ± 1.1 nM) was observed using a picogreen assay. The biochemical data were further supported by crystallographic studies via co-crystallization of Cmpd I with the RT protein. The crystal structure (PDB ID code 6OE3) had a resolution of 2.90 Å and exhibited a monoclinic symmetry in space group *C* 2 with one heterodimer in the asymmetric unit. Table 2 shows the data collection, processing and refinement statistics of RT:Cmpd I structure. The overall structure was similar to one of the previously described naphthyl catechol phenyl ether inhibitors (Kudalkar et al., 2017). The Cmpd I was deeply buried in the open NNRTI binding pocket (NNBP) and made extensive contacts with the residues in the non-nucleoside binding pocket (NNBP) (Fig. 2A). The naphthyl moiety of Cmpd I was located in the hydrophobic region of NNBP and was stabilized by several van der Waals interactions with P95, L100, V108, Y188, W229, F227 and L234. Additionally, the naphthyl ring formed a π-π stacking interaction with Y188 and W229 residues. The nitrile group of the naphthyl ring resides in the tunnel region close to the polymerase active site. The central catechol ring is stabilized via π-π interaction with Y181. The uracil moiety is anchored in the groove region of the NNBP via π-π interaction with Y318 and its 2-carbonyl group is in H-bond distance with the amino group of the side chain of K102 (3.5 Å) and with the amide of the backbone of K103 and P236 (3.3 Å and 3.4 Å Fig. 2B).

The cellular anti-HIV activity of Cmpd I against WT RT is shown in Table 1 and is compared to FDA approved NNRTIs; rilpivirine and efavirenz (Fig. 1). Cmpd I showed single digit nanomolar EC_{50} (1.1 nM) against WT RT in the cell based assays suggesting high potency (Lee et al., 2014). The solubility of Cmpd I was 9.1 μg/ml, which was > 100-fold greater that for rilpivirine and within 8-fold the value determined

Table 2
Data collection and refinement statistics for RT (WT) in the complex with Cmpd I.

PDB ID code [a]	6OE3
(A) Data collection and processing	
Wavelength (Å)	0.9791
space group	C2
unit cell parameters a, b, c, (Å);	226.5, 69.9, 105.0;
α, β,γ, (°)	90.0, 105.2, 90.0;
Matthews coefficient [b] ($Å^3$/Da)	3.45
solvent content [b] (%)	64.4
(B) Diffraction data	
resolution range (Å)	50–2.90 (3.07–2.90)
unique reflections	34181 (5280)
R(I)sym (%)	9.0 (109.8)
Wilson B factor (Å2)	18.2
completeness (%)	97.8 (94.7)
redundancy	3.1 (2.7)
< I/σ(I) >	11.5 (1.1)
CC(1/2)	99.6 (63.2)
(C) Refinement	
resolution range (Å)	43.17-2.90
reflections used in refinement (work/free)	32471/1709
final R value for all reflections (work/free) (%)	0.23/0.27
protein residues (chain A/B)	546/409
water molecules	8
RMSD from ideality: bond lengths (Å)	0.006
RMSD from ideality: bond angles (°)	0.821
Ramachandran plot[c]:	
residues in most favored regions (%)	92.8
residues in additionally allowed regions (%)	6.7
residues in generously allowed regions (%)	0.2
residues in disallowed regions (%)	0.2
Mean *B* factor protein ($Å^2$) [d]	91.5
Mean *B* factor ligand ($Å^2$) [d]	67.8
Mean *B* factor water molecules ($Å^2$) [d]	59.7

[a] Values in parenthesis describe the highest resolution shell.
[b] Calculated with Matthews_coef program from CCP4 suite version 7.0.053 (Matthews, 1968).
[c] Calculated with PROCHECK (Laskowski et al., 1993).
[d] Mean B factors were calculated with MOLEMAN (Kleywegt et al., 2001).

for efavirenz. The CLogP value of 3.59 of Cmpd I was in the normal range of 0–5 for oral drugs (Jorgensen, 2009) while for efavirenz, it was 4.6 and for rilpivirine it was above 5 (Bollini et al., 2013; Jorgensen, 2009; Jorgensen and Duffy, 2002; Lee et al., 2014; Lee et al., 2013). The cytotoxic concentration (CC_{50}) for Cmpd I was > 100 μM providing a therapeutic index of > 100,000 whereas efavirenz and rilpivirine were cytotoxic to cells at a lower concentration range of 8–15 μM. The potent intrinsic inhibitory activity, better solubility profile, and low ClogP values of Cmpd I compared to rilpivirine (Janssen et al., 2005; Sun et al., 2012) and efavirenz (Frey et al., 2014; Lee et al., 2013) suggests that Cmpd I is a good drug candidate for further preclinical evaluation.

Additionally, Cmpd I was characterized along with efavirenz utilizing in vitro pharmacological profiling assays in order to identify any off-target effects. A panel of 34 targets including various ion channels, receptors, hormones and enzymes were used. The significant response from each assay is plotted as a heat map (Fig. 3). No adverse response was observed for Cmpd I to any of the targets tested except for an isoform cytochrome P450 2C19(CYP2C19) where a little over 50% response was seen. This CYP2C subfamily is responsible for metabolizing ~20% of marketed drugs (Goldstein, 2001). Notably, Cmpd I did not hit any major targets like the hERG channel, blockade of which is responsible for major cardiac arrhythmias (Bowes et al., 2012). Additionally, no adverse reaction was seen against CYP3A4, the major cytochrome P450 enzyme responsible for the metabolism of the majority of currently approved drugs (Nazir et al., 2016; Wang et al., 2016). In contrast, inhibition of binding of ligands to DHP and Na channels and 5HT2B receptors were observed with efavirenz suggesting that these might contribute to some of the side effects seen with efavirenz treatment.

The excellent in vitro pharmacological qualities of Cmpd I led us to develop a nanoformulation of Cmpd I (Cmpd I-NP) and explore the in vivo pharmacokinetics of both free and nanoformulated Cmpd I in BALB/c mice. Cmpd I-loaded PLGA based nanoparticles (Cmpd I-NP) were made using emulsion-solvent evaporation technique as described in methods (Le Thi Mai et al., 2009). Characterization of Cmpd I showed that it was encapsulated in PLGA with an average diameter of 320 ± 38 nm, polydispersity index (PDI) of 0.15 ± 0.1, and an average negative zeta potential of −24 ± 0.9 mV. Representative scanning electron microscope (SEM) images illustrated that Cmpd I-NP exhibited spherical shapes (Fig. 4) and the size estimates from SEM were consistent with the size of Cmpd I-NP reported by DLS. The diameter of the Cmpd I-NP were in the range that has been previously reported to avoid clogging of the lymphatic ducts and fine capillaries (Bose et al., 2014). Additionally, the slightly negative surface charge suggests that the nanoparticles will be less cytotoxic and will have prolonged circulation time in vivo by escaping uptake in cells and tissues (Jiang et al., 2015; Zhang et al., 2008). A theoretical drug loading of 10 wt% was input into the nanoparticle synthesis; the drug loading (DL%) in the formulated mixture was of 10 ± 0.7 wt% resulting in an encapsulation efficiency (EE) of 100 ± 7%.

To determine the delivery and sustainability in vivo, free Cmpd I and Cmpd I-NP were injected into BALB/c mice, and the persistence of Cmpd I in the circulation was measured. The mice were divided into two groups of three mice each where one group received a single dose of Cpmd I (100 mg/kg) and the second group received 125 mg/kg dose of Cmpd I in the form of nanoforumlation, intraperitoneally. The blood

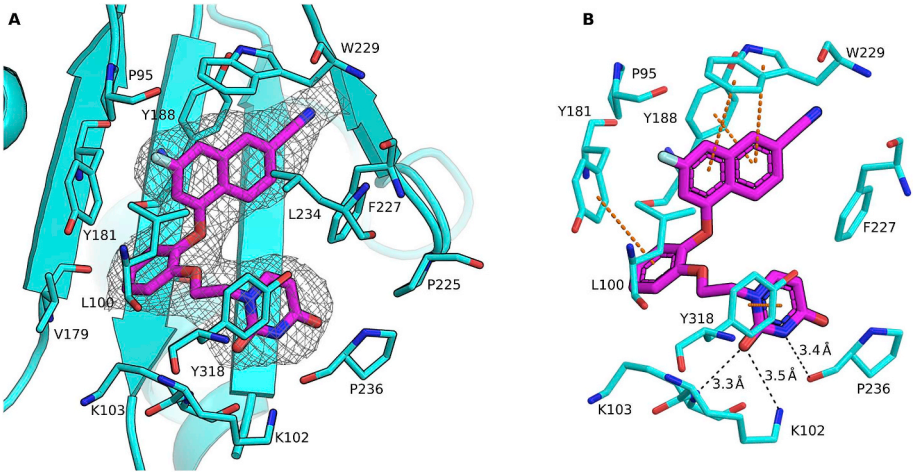

Fig. 2. Close-up views of NNBP of the crystal structures of RT in complexes with NNRTI: Cmpd I (PDB code: 6OE3). The protein is displayed in cyan. The carbon atoms of Cmpd I are shown in magenta. Cmpd I is shown as stick model. (A) The protein is represented as ribbon model and the amino acids within a distance of 5 Å are shown as stick model. *Fo-Fc* polder electron density map is shown as gray mesh at a contour level of 4 σ. (B) Close-up view on the binding mode of compound I. H-bond interactions are depicted as black dotted lines. Distances are given in Å. π-π stacking interactions are depicted as orange dotted line. All structural representations were prepared with PyMOL. (The PyMOL Molecular Graphics System).

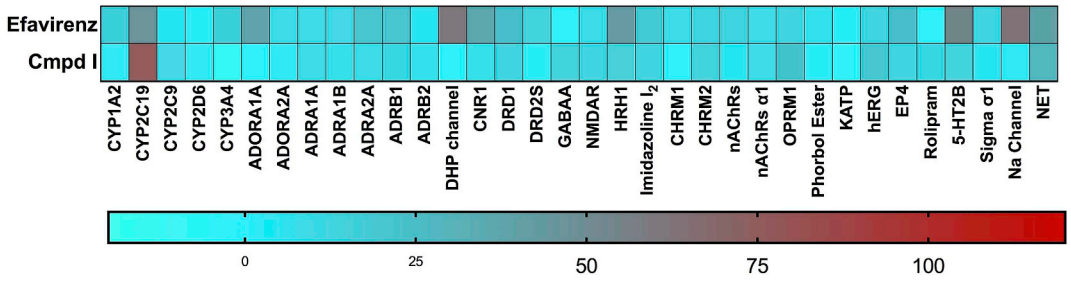

Fig. 3. In-vitro pharmacological profiling of efavirenz, and Cmpd I against targets for adverse drug reactions (ADRs). Rows represent compounds tested and columns represent targets. Percentage inhibition at 10 μM concentration of the compounds is color-coded. CYP, cytochrome P450, ADOR, Adenosine receptor, ADR, adrenergic receptor, DHP, dihydropyridine or calcium channel L-type, CNR1, cannabinoid receptor, DRD, Dopamine receptor, NMDAR, Glutamate receptor, HRH1, Histamine receptor, Imidazole I2, Imidazole I2 receptor, CHRM, Muscarinic, nACHR, nicotinic acetylcholine, OPRM, opiate μ, Phorbol ester receptor, KATP, potassium channel, hERG, the human Ether-à-go-go-Related Gene, EP4, prostanoid receptor, Rolipram, phosphodiesterase-4 inhibitor, 5HT2B, serotonin receptor 2B, Sigma σ1 receptor, Na channel, sodium channel, NET, norepinephrine transporter.

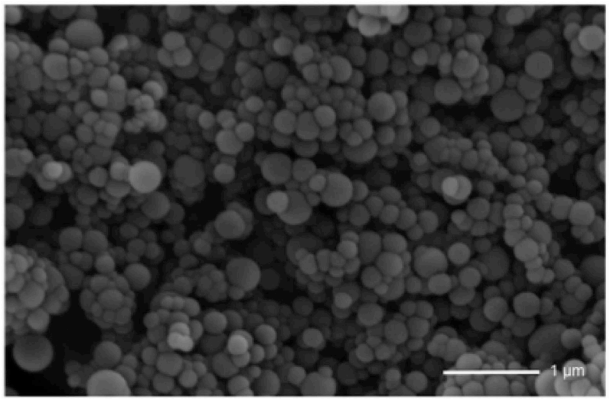

Fig. 4. Scanning electron microscopy (SEM) of fabricated antiviral nanoparticles. The PLGA nanoparticles were loaded with Cmpd I as described in Methods.

samples were collected over a period of time until Cmpd I reached undetectable levels in both groups.

The serum concentration as a function of time after a single i.p. dose of Cmpd I showed that Cmpd I was rapidly absorbed, achieving a maximum concentration (C_{max}) of 7.8 ± 0.9 μg/ml at 8 h; this concentration is 10,000-fold higher, than the therapeutic/effective concentrations (EC_{50}) (Fig. 5A). The plasma concentration of Cmpd I remained near this level for ~36 h than decreased to undetectable levels by 72 h. A slightly lower C_{max} of 5.2 ± 1.6 μg/ml was observed at 48 h for Cmpd I-NP (Fig. 5B). However, Cmpd I was detected in serum for 30 days after a single i.p. dose of the nanoformulation. Importantly, the observed serum concentration of 1.7 μg/ml for Cmpd I-NP at day 30 was substantially greater (> 3000-fold) than the EC_{50} for the wild-type HIV-1 in the MT-2 assay (Fig. 5C) (Lee et al., 2013).

Table 3 shows the PK parameters of Cmpd I and Cmpd I-NP in BALB/c mice. The $AUC_{0\text{-last}}$ (1004 ± 60.45μg/ml/h) for Cmpd I injected as the nanoformulation was 2.3 times higher and the clearance

Table 3
Pharmacokinetic parameters of Cmpd I and Cmpd I-NP following ip injection in BALB/c mice. Data are the mean ± S.D. values of triplicate measurement; n represents the number of mice.

Pharmacokinetic Parameters	Cmpd I (n = 3)	Cmpd I-NP (n = 3)
Dose (mg/kg)	100	125
C_{max} (μg/ml)	7.8 ± 0.9	5.2 ± 1.6
T_{max} (h)	8	48
$AUC_{0\text{-last}}$ (μg h/ml)	431.9 ± 27.3	1004 ± 60.45
CL (ml/min/kg)	3.9	2.0

rate (CL 2.0 ml/min/kg) was ~2 times lower than free injected Cmpd I ($AUC_{0\text{-last}}$ 431.9 ± 27.3 μg/ml/h and CL 3.9 ml/min/kg). In Fig. 5D the serum levels for first 72 h are superimposed to highlight the differences in distribution and clearance over time between free Cmpd I and Cmpd I-NP. The larger AUC_{0-last} values and lower CL value for Cmpd I-NP could suggest that a higher volume of distribution can be achieved by nanoformulation of Cmpd I and it is subjected to slower metabolism to maintain long-lasting serum levels. The longer residence time of Cmpd I in the serum when administered as Cmpd I-NP compared to the free drug can be attributed to a number of factors including slow release of Cmpd I from the polymer nanoparticle directly into body fluids and/or the cellular uptake of the particles followed by the slow release of the Cmpd I from intracellular breakdown of the polymer.

The serum samples collected at specified time were further analyzed for antiviral potency in an assay using TZM-bl indicator cell line infected with HIV. This cell line expresses a luciferase reporter driven by the HIV long terminal repeats and thus provides a linear measure for HIV infection (Kudalkar et al., 2017). The assay was carried out as described in the methods section and > 97% inhibition was observed in serum samples collected as early as 2 h post-administration of Cmpd I and Cmpd I-NP (Fig. 6). This level of inhibition was maintained till day 2 for free compound I and day 30 for Cmpd I-NP suggesting that the levels of Cmpd I in both groups (free or nanoformulated) were higher

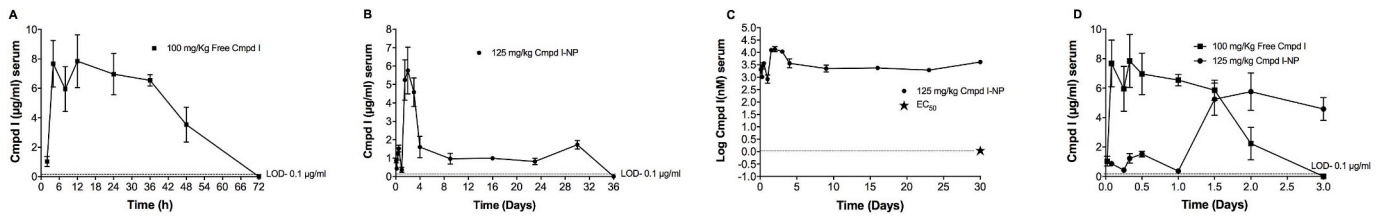

Fig. 5. Pharmacokinetics of Cmpd I and Cmpd I-NP in BALB/c mice. The serum levels of Cmpd I after i.p. administration of 100 mg/kg of free Cmpd I (A) and 125 mg/kg of Cmpd I-NP (B). The blood samples were collected at different intervals and analyzed as described in Methods. Data points represent mean ± SD. (C) The log of serum concentrations for Cmpd I-NP were plotted against time and compared to EC_{50} (★)- 1.1 nM. Note the > 3 log difference between serum concentration and EC_{50}. (D) The serum levels of free Cmpd I and Cmpd I-NP are superimposed for the first 72 h to show the difference in Cmpd I distribution.

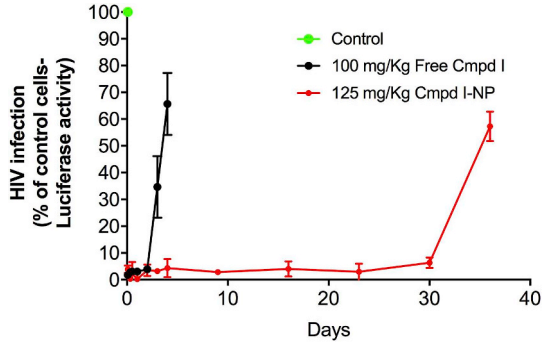

Fig. 6. HIV-1 inhibition by serum containing Cmpd I and Cmpd I-NP in TZM-bl cells. TZM-bl cells presented with serum containing Cmpd I or Cmpd I-NP collected at different intervals as described in Methods, were infected with HIV-1 (JRCSF strain). Virus infection was measured 2 days later by measuring luciferase activity in the cells. The percentage of the luciferase activity was normalized relative to the HIV-1 infected control TZM-bl cells that were not exposed to Cmpd I or Cmpd I-NP. The values are mean ± SD.

than the effective therapeutic concentrations and will be sufficient to control the HIV-infection in our future efficacy studies.

In conclusion, we have discovered a new HIV-1 NNRTI that exhibits significant antiviral activity and has favorable in vitro pharmacological characteristics. The data presented in this study further showed that the effective therapeutic concentrations of Cmpd I can be achieved in mice administered with free or nanoformulated Cmpd I. Additionally, all the mice appeared healthy with no signs of morbidity or mortality throughout the study. Furthermore, the nanoformulation of Cmpd I provided a slow and sustained release of compound I in BALB/c mice and the levels of Cmpd I were maintained well above the required therapeutic levels for a month even after a single dose. Given the favorable in vitro and in vivo profile of Cmpd I the next logical step is to measure the therapeutic potential of free and nanoformulated Cmpd I in an animal model of HIV infection.

Author contributions

K.S.A., W.L.J., W.M.S., P.K., and S.N.K. designed research; S.N.K., I.U., N.B., J.B., H.K.M., E.Q., K.A.S., and J.A.C. performed research; S.N.K., N.B., H.K.M., and J.A.C. analyzed data; and S.N.K., N.B., H.K.M., K.S.A., W.L.J., W.M.S., and P.K. wrote the paper.

Acknowledgements

This work was supported by grants from the National Institutes of Health [Grants AI044616, GM049551, AI141172, AI112443, AI122384, and EB000487]. Crystals screening was conducted with support from the Yale Macromolecular X-ray Core Facility [1S10OD018007-01]. This research used resources of the Advanced Photon Source, a U.S. Department of Energy (DOE) Office of Science User Facility operated for the DOE Office of Science by Argonne National Laboratory under Contract No. DE-AC02-06CH11357. This work is based upon research conducted at the Northeastern Collaborative Access Team beamlines, which are funded by the National Institute of General Medical Sciences from the National Institutes of Health (P30 GM124165). The Eiger 16M detector on 24-ID-E beam line is funded by a NIH-ORIP HEI grant (S10OD021527).

References

Adams, P.D., et al., 2010. PHENIX: a comprehensive Python-based system for macromolecular structure solution. Acta Crystallogr. Sect. D Biol. Crystallogr. 66, 213–221. https://doi.org/10.1107/S0907444909052925.

Bollini, M., et al., 2013. Optimization of diarylazines as anti-HIV agents with dramatically enhanced solubility. Bioorg. Med. Chem. Lett 23, 5213–5216. https://doi.org/10.1016/j.bmcl.2013.06.091.

Bose, T., Latawiec, D., Mondal, P.P., Mandal, S., 2014. Overview of nano-drugs characteristics for clinical application: the journey from the entry to the exit point. J. Nanoparticle Res. 16, 2527.

Bourget, P., Delouis, J.M., 1993. [Review of a technic for the estimation of area under the concentration curve in pharmacokinetic analysis]. Therapie 48, 1–5.

Bowes, J., et al., 2012. Reducing safety-related drug attrition: the use of in vitro pharmacological profiling. Nat. Rev. Drug Discov. 11, 909–922. https://doi.org/10.1038/nrd3845.

Collaborative Computational Project, N., 1994. The CCP4 suite: programs for protein crystallography. Acta Crystallogr D Biol Crystallogr 1, 760–763.

Das, K., et al., 2008. High-resolution structures of HIV-1 reverse transcriptase/TMC278 complexes: strategic flexibility explains potency against resistance mutations. Proc. Natl. Acad. Sci. U. S. A. 105 (5), 1466–1471.

de Waal, R., et al., 2013. Systematic review of antiretroviral-associated lipodystrophy: lipoatrophy, but not central fat gain, is an antiretroviral adverse drug reaction. PLoS One 8, e63623. https://doi.org/10.1371/journal.pone.0063623.

Delaugerre, C., et al., 2001. Resistance profile and cross-resistance of HIV-1 among patients failing a non-nucleoside reverse transcriptase inhibitor-containing regimen. J. Med. Virol. 65, 445–448.

Emsley, P., Cowtan, K., 2004. Coot: model-building tools for molecular graphics. Acta Crystallogr. Sect. D Biol. Crystallogr. 60, 2126–2132. https://doi.org/10.1107/S0907444904019158.

Emsley, P., et al., 2010. Features and development of Coot. Acta Crystallogr. Sect. D Biol. Crystallogr. 66, 486–501. https://doi.org/10.1107/S0907444910007493.

Frey, K.M., et al., 2012. Crystal structures of HIV-1 reverse transcriptase with picomolar inhibitors reveal key interactions for drug design. J. Am. Chem. Soc. 134, 19501–19503. https://doi.org/10.1021/ja3092642.

Frey, K.M., et al., 2014. Structure-based evaluation of C5 derivatives in the catechol diether series targeting HIV-1 reverse transcriptase. Chem. Biol. Drug Des. 83, 541–549. https://doi.org/10.1111/cbdd.12266.

Gao, Y., Kraft, J., Yu, D., Ho, R.J., 2018. Recent developments of nanotherapeutics for targeted and long-acting, combination HIV chemotherapy. Eur. J. Pharm. Biopharm. https://doi.org/10.1016/j.ejpb.2018.04.014. https://doi.org/10.1016/j.ejpb.2018.04.014.

Goldstein, J.A., 2001. Clinical relevance of genetic polymorphisms in the human CYP2C subfamily. Br. J. Clin. Pharmacol. 52, 349–355.

Gray, W.T., et al., 2015. Potent inhibitors active against HIV reverse transcriptase with K101P, a mutation conferring rilpivirine resistance. ACS Med. Chem. Lett. 6, 1075–1079. https://doi.org/10.1021/acsmedchemlett.5b00254 http://www.Molinspiration.com.

Huang, B., et al., 2015. Fused heterocycles bearing bridgehead nitrogen as potent HIV-1 NNRTIs. Part 3: optimization of [1,2,4]triazolo[1,5-a]pyrimidine core via structure-based and physicochemical property-driven approaches. Eur. J. Med. Chem. 92, 754–765. https://doi.org/10.1016/j.ejmech.2015.01.042.

Janssen, P.A., et al., 2005. In search of a novel anti-HIV drug: multidisciplinary coordination in the discovery of 4-[[4-[[4-[(1E)-2-cyanoethenyl]-2,6-dimethylphenyl]amino]-2- pyrimidinyl]amino]benzonitrile (R278474, rilpivirine). J. Med. Chem. 48, 1901–1909.

Jiang, Y., et al., 2015. Nanoparticle-based ARV drug combinations for synergistic inhibition of cell-free and cell-cell HIV transmission. Mol. Pharm. 12, 4363–4374. https://doi.org/10.1021/acs.molpharmaceut.5b00544.

Jorgensen, W.L., 2009. Efficient drug lead discovery and optimization. Acc. Chem. Res. 42, 724–733. https://doi.org/10.1021/ar800236t.

Jorgensen, W.L., Duffy, E.M., 2002. Prediction of drug solubility from structure. Adv. Drug Deliv. Rev. 54, 355–366.

Kabsch, W., 2010. Xds. Acta Crystallogr. Sect. D Biol. Crystallogr. 66, 125–132. https://doi.org/10.1107/S0907444909047337.

King, R.W., et al., 2002. Potency of nonnucleoside reverse transcriptase inhibitors (NNRTIs) used in combination with other human immunodeficiency virus NNRTIs, NRTIs, or protease inhibitors. Antimicrob. Agents Chemother 46, 1640–1646. https://doi.org/10.1128/AAC.46.6.1640-1646.2002.

Kleywegt, G.J., Zhou, J.Y., Kjeldgaard, M., Jones, T.A., 2001. International Tables for Crystallography, Volume F. Crystallography of Biological Macromolecules.

Kohlstaedt, L.A., et al., 1992. Crystal structure at 3.5 A resolution of HIV-1 reverse transcriptase complexed with an inhibitor. Science 256, 1783–1790.

Kudalkar, S.N., et al., 2017. Structural and preclinical studies of computationally designed non-nucleoside reverse transcriptase inhibitors for treating HIV infection. Mol. Pharmacol. 91, 383–391. https://doi.org/10.1124/mol.116.107755.

Kudalkar, S.N., et al., 2018. From in silico hit to long-acting late-stage preclinical candidate to combat HIV-1 infection. Proc. Natl. Acad. Sci. U. S. A. 115, E802–E811. https://doi.org/10.1073/pnas.1717932115.

Laskowski, R. a., MacArthur, M.W., Moss, D.S., Thornton, J.M., 1993. PROCHECK: a program to check the stereochemical quality of protein structures. J. Appl. Crystallogr. 26, 283–291.

Le Thi Mai, H., et al., 2009. Preparation of drug nanoparticles by emulsion evaporation method. J. Phys. Conf. Ser. 187, 012047.

Lee, W.G., et al., 2016. Design, conformation, and crystallography of 2-naphthyl phenyl ethers as potent anti-HIV agents. ACS Med. Chem. Lett. 7, 1156–1160. https://doi.org/10.1021/acsmedchemlett.6b00390.

Lee, W.G., et al., 2014. Picomolar inhibitors of HIV-1 reverse transcriptase: design and crystallography of naphthyl phenyl ethers. ACS Med. Chem. Lett. 5, 1259–1262. https://doi.org/10.1021/ml5003713.

Lee, W.G., et al., 2015. Discovery and crystallography of bicyclic arylaminoazines as potent inhibitors of HIV-1 reverse transcriptase. Bioorg. Med. Chem. Lett 25, 4824–4827. https://doi.org/10.1016/j.bmcl.2015.06.074.

Lee, W.G., et al., 2013. Picomolar inhibitors of HIV reverse transcriptase featuring bicyclic replacement of a cyanovinylphenyl group. J. Am. Chem. Soc. 135, 16705–16713. https://doi.org/10.1021/ja408917n.
Mandal, S., Kang, G., Prathipati, P.K., Fan, W., Li, Q., Destache, C.J., 2018. Long-acting parenteral combination antiretroviral loaded nano-drug delivery system to treat chronic HIV-1 infection: a humanized mouse model study. Antivir. Res. 156, 85–91. https://doi.org/10.1016/j.antiviral.2018.06.005.
Matthews, B.W., 1968. Solvent content of protein crystals. J. Mol. Biol. 33, 491–497.
McCoy, A.J., et al., 2007. Phaser crystallographic software. J. Appl. Crystallogr. 40, 658–674. https://doi.org/10.1107/S0021889807021206.
Moriarty, N.W., et al., 2009. Electronic Ligand Builder and Optimization Workbench (eLBOW): a tool for ligand coordinate and restraint generation. Acta Crystallogr. Sect. D Biol. Crystallogr. 65, 1074–1080. https://doi.org/10.1107/S0907444909029436.
Morin, A., et al., 2013. Collaboration gets the most out of software. eLife 2, e01456. https://doi.org/10.7554/eLife.01456.
Nazir, S., et al., 2016. Variation in pharmacokinetics of omeprazole and its metabolites by gender and CYP2C19 genotype in Pakistani male and female subjects. Pak. J. Pharm. Sci. 29, 887–894.
Ratain, M.J., Plunkett, W.K., 2003. Principles of pharmacokinetics. In: Kufe DW, P.R., Weichselbaum, R.R. (Eds.), Holland-frei Cancer Medicine, sixth ed. Hamilton (ON).
Rhee, S.-Y., et al., 2015. Geographic and temporal trends in the molecular epidemiology and genetic mechanisms of transmitted HIV-1 drug resistance: an individual-patient- and sequence-level meta-analysis. PLoS Med. 12, e1001810. https://doi.org/10.1371/journal.pmed.1001810.
Riddler, S.A., et al., 2008. Class-sparing regimens for initial treatment of HIV-1 infection. N. Engl. J. Med. 358, 2095–2106. https://doi.org/10.1056/NEJMoa074609.
Smart, O.S.W., T.O., Sharff, A., Flensburg, C., Keller, P., Paciorek, W., Vonrhein, C., Bricogne, G., 2011. http://www.globalphasing.com.
Sun, L.Q., et al., 2012. Optimization of 2,4-diarylanilines as non-nucleoside HIV-1 reverse transcriptase inhibitors. Bioorg. Med. Chem. Lett 22, 2376–2379. https://doi.org/10.1016/j.bmcl.2012.02.055.
The PyMOL Molecular Graphics System, V. x. S., LLC..
Wang, Y., et al., 2016. Association between CYP2C19 loss-of-function allele status and efficacy of clopidogrel for risk reduction among patients with minor stroke or transient ischemic attack. JAMA 316, 70–78. https://doi.org/10.1001/jama.2016.8662.
Zhang, Y., et al., 2008. Zeta potential: a surface electrical characteristic to probe the interaction of nanoparticles with normal and cancer human breast epithelial cells. Biomed. Microdevices 10, 321–328. https://doi.org/10.1007/s10544-007-9139-2.